Glenthenamines A–F: Enamine pyranonaphthoquinones from the Australian pasture plant-derived *Streptomyces* sp. CMB-PB042

Taizong Wu,[†] Angela A. Salim,[†] Hui Cui,[§] Zeinab G. Khalil,[†] Paul V. Bernhardt[‡], and Robert J. Capon[†*]

[†]Institute for Molecular Bioscience, The University of Queensland, Brisbane, QLD 4072, Australia

[‡]School of Chemistry and Molecular Bioscience, The University of Queensland, Brisbane, QLD 4072, Australia

[§]School of Pharmaceutical Sciences, Guangzhou University of Chinese Medicine, Guangzhou, 510006, China

*corresponding author r.capon@uq.edu.au

ABSTRACT

Chemical investigations into solid phase cultivations of an Australian sheep station pasture plant-derived *Streptomyces* sp. CMB-PB042, yielded the rare enamine naphthopyranoquinones BE-54238A (**1**) and BE-54238B (**2**), together with four new analogues, glenthenamines B–D (**4–6**) and F (**8**), and two handling artifacts, glenthenamines A (**3**) and E (**7**). Single crystal X-ray analyses of **1–2** resolved configurational ambiguities in the scientific literature, while detailed spectroscopic analysis and biosynthetic considerations assigned structures inclusive of absolute configuration to **3–8**. We propose a plausible sequence of biosynthetic transformations linking structural and configurational features of **1–8**, and apply a novel Schiff base "fishing" approach to detect a key deoxyaminosugar precursor. These enamine naphthopyranoquinone disclose a new P-gp inhibitory pharmacophore capable of reversing doxorubicin resistance in P-gp overexpressing colon carcinoma cells.

As part of our ongoing investigation into new and unusual natural products produced by Australian microbes, we assembled a library of bacterial and fungal isolates from Australia sheep station pasture soils and plants, with solvent extracts of agar plate cultivations subjected to biological and chemical profiling. Based on this strategy, our attention was drawn to *Streptomyces* sp. CMB-PB042 isolated from a pasture plant collected near Glenthompson in the southwest of Victoria, Australia. More specifically, the EtOAc extract of an ISP2 agar plate cultivation of CMB-PB042 inhibited motility of *Dirofilaria immitis* microfilariae (EC_{50} 0.7 μg/mL), a parasitic roundworm transmitted by mosquito, and responsible for serious lung disease, heart failure and death in companion animals, particularly dogs. The paucity of current treatment options for *D. immitis* infections prompted us to explore the chemistry of CMB-PB042 further.

RESULTS AND DISCUSSION

Scaled-up ISP2 solid phase cultivation of CMB-PB042, followed by solvent extraction, trituration, and reversed phase chromatography yielded the antiparasitic fraction as a complex mixture of polyether ionophores, including the known metabolite nigericin (Table S1). Polyether ionophores were particularly evident in the GNPS molecular networking analysis[1] of the extract and derived fractions, as both M+Na and $M+NH_4$ clusters, with the presence of nigericin confirmed by co-clustering with an authentic sample (Figure S5). Although nigericin proved to be a potent inhibitor of *D. immitis* microfilariae motility (EC_{50} 0.07 μM), in our assessment polyether ionophores are not a useful starting point for developing new treatments for *D. immitis*.

Notwithstanding, chemical profiling of other (inactive) CMB-PB042 fractions revealed a noteworthy GNPS family of non-polyether metabolites (Figure S5) featuring molecular formulae not well represented in the natural products literature. To better understand the production of these metabolites we employed a media MATRIX microbioreactor approach to trial 12 different media compositions under solid phase as well as static and shaken broth (36 conditions).[2] This analysis confirmed that a combination of both ISP2 and M2 solid phase cultivations provide optimal coverage of the target GNPS family (Figure S6). Further fractionation of the ISP2 solid phase cultivation extract yielded **1–5** and **7–8**, while fractionation of a scaled up M2 solid phase cultivation yielded the additional analogue **6**. What follows is an account of the structure elucidation of **1–8** based on detailed spectroscopic analysis and biosynthetic considerations.

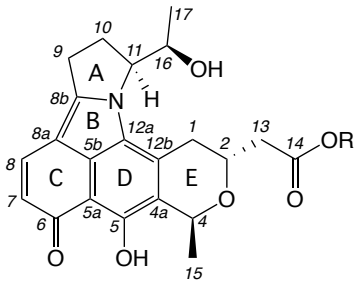

(**1**) R = H
(**3**) R = CH_3

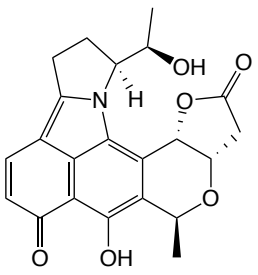

(**2**)

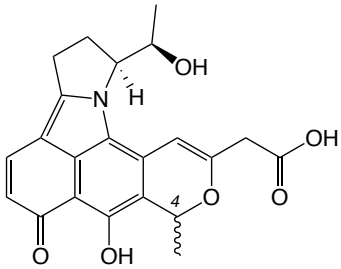

(**4**) 4*S*
(**5**) 4*R*

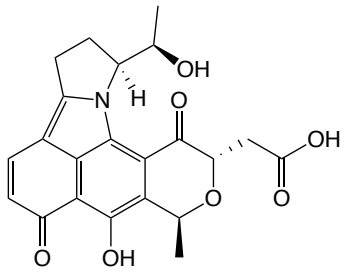

(**6**)

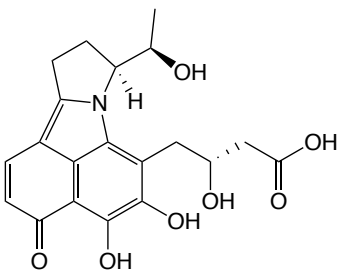

(**7**)

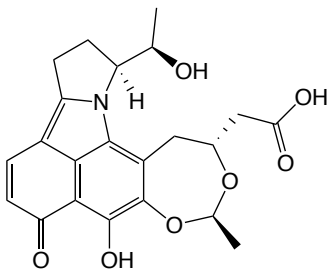

(**8**)

HRESI(+)MS measurements on **1** and **2** revealed molecular formulae ($C_{22}H_{23}NO_6$, Δmmu +1.7 and $C_{22}H_{21}NO_6$, Δmmu +2.4), which together with UV-vis and 1D NMR (DMSO-d_6) data (Tables S3–S4, Figures S7–S8 and S13–S14) were consistent with the

rare enamino-pyranonaphthoquinones BE-54238A and BE-54238B, respectively. First isolated from the Japanese soil *Streptomyces* sp. A54238, **1–2** were patented as potential anticancer agents in 1998,[3] with the planar structures reported in the scientific literature in 2000 (*sans* optical rotations).[4] While an asymmetric synthesis provided the absolute configuration for **2** (1*S*,2*S*,4*S*,11*S*,16*R*) ($[\alpha]_D$ -521) in 2004,[5] no optical measurements or configurational assignments have been reported for **1**, even though it appears in a 2005 literature review with a 2*R*,4*S*,11*S*,16*R* configuration (presumably based on biosynthetic comparisons to **2**).[6] The *Streptomyces* metabolites **1–2** remain the sole exemplars of this rare enamine pyranonaphthoquinone scaffold. A rediscovery in 2017 from the Chinese soil *Streptomyces* sp. MBT76 prompted investigation into the relevant biosynthetic gene cluster, however, despite presenting no spectroscopic or optical data, or structure elucidation arguments, these latter authors also present alternate relative/absolute configurations for both **1** (2*S*,4*R*,11*R*,16*R*) and **2** (1*R*,2*R*,4*R*,11*R*,16*R*).[7]

In an effort to resolve the resulting configurational ambiguities in the scientific literature we used 2D NMR (DMSO-d_6) and single crystal X-ray diffraction to determine relative and absolute configurations for our *Streptomyces* sp. CMB-PB042 re-isolations of **1** ($[\alpha]_D$ -385, MeOH) and **2** ($[\alpha]_D$ -323, MeOH) (Tables S3–S4, Figures 1–3 and S7–S18). Compound **1** was crystallized as **1**·MeCN·H_2O and compound **2** as its hemihydrate. The absolute configurations of compounds **1** and **2** were established by the method of Hooft *et al.*[8] comprising analysis of 1618 and 1212 Bijvoet pairs, respectively. The carboxymethyl substituent of **1** was disordered over two positions. These X-ray analyses re-affirmed the absolute configuration assigned by total synthesis in 2004.

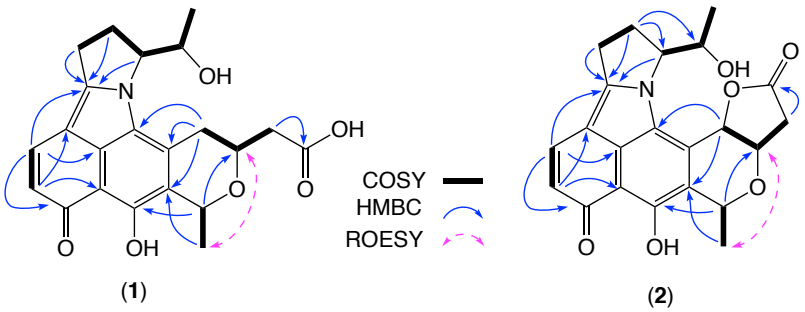

(1) (2)

Figure 1. Selected 2D NMR (DMSO-d_6) correlations for **1** and **2**.

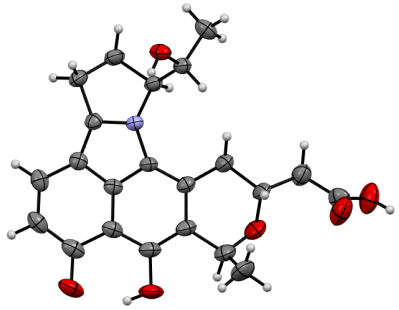

Figure 2. X-ray crystal structure for **1**.

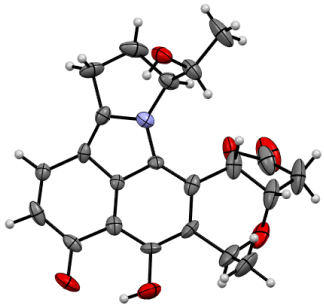

Figure 3. X-ray crystal structure for **2**.

HRESI(+)MS measurements on **3** revealed a molecular formula ($C_{23}H_{25}NO_6$, Δmmu +2.2) consistent with a CH_2 homologue of **1**, with NMR (DMSO-d_6) data revealing the principal difference as replacement of the CO_2H moiety in **1** with a CO_2CH_3 moiety in **3** (δ_H 3.66, s, $CO_2C\underline{H}_3$; δ_C 51.4, $CO_2\underline{C}H_3$), confirmed by diagnostic HMBC correlations (Tables 1–2 and S5, Figures 4 and S19–S24). Based on biogenetic considerations, glenthenamine A (**3**) ($[\alpha]_D$ -254, MeOH) was assigned an absolute configuration in common with co-metabolites **1–2**.

HRESI(+)MS measurements on **4** and **5** revealed molecular formula ($C_{22}H_{21}NO_6$, Δmmu +2.6 and +2.5, respectively) consistent with isomeric didehydro analogues of **1**. Comparison of the NMR (DMSO-d_6) data for **4** and **5** with **1** revealed the principal differences as replacement of resonances for C-1/H_2-1 and C-2/H-2 in **1**, with those attributed to a Δ^1 in **4** (δ_H 6.13, br s, H-1; δ_C 97.3, C-1; 154.9, C-2) and **5** (δ_H 6.23, br s, H-1; δ_C 98.2, C-1; 154.5, C-2), further confirmed by diagnostic HMBC correlations (Tables 1–2 and S6–S7, Figures 4 and S25–S36). Having established that **4** and **5** were diastereomers, excellent concordance across 1D NMR resonances for ring A was suggestive of a common C-11/C-16 relative configuration. Even though the specific rotation for **4** ($[\alpha]_D$ -567, MeOH) differed significantly from that of **5** ($[\alpha]_D$ -40, MeOH), this alone did not provide evidence for an assignment of absolute configuration. This determination was achieved by comparison of experimental versus calculated ECD spectra, which indicated that **4** and **5** were most likely C-4 epimers, with **4** possessing a 4*S* configuration (in common with **1**) (Figures 5 and Supporting Information Sections 7-8). Of note, the C-4 configuration in **4** and **5** had a profound impact on the 350 nm Cotton effect, most likely due to n-π* transition between oxygen and the double bond. Thus, structures for glenthenamines B (**4**) and C (**5**) were assigned as shown, with absolute configurations in accord with co-metabolites **1–2**.

HRESI(+)MS measurements on **6** revealed a molecular formula ($C_{22}H_{21}NO_7$, Δmmu +1.0) consistent with an oxidized analogue of **1**. Comparison of the NMR (DMSO-d_6) data for **6** with **1** revealed the principal difference as transformation of the C-1 methylene in **1** into a ketone in **6** (δ_C 194.9, C-1), with the planar structure confirmed by diagnostic

2D NMR correlations (Tables 1–2 and S8, Figures 4 and S37–S42). High levels of concordance across the ^{13}C NMR data for **6** with **1** about ring A, and a ROESY correlation between H-2 and H-4, supported a relative configuration in common with **1**. Based on biogenetic considerations glenthenamine D (**6**) ($[\alpha]_D$ -265, MeOH) was assigned an absolute configuration in common with co-metabolites **1–2**.

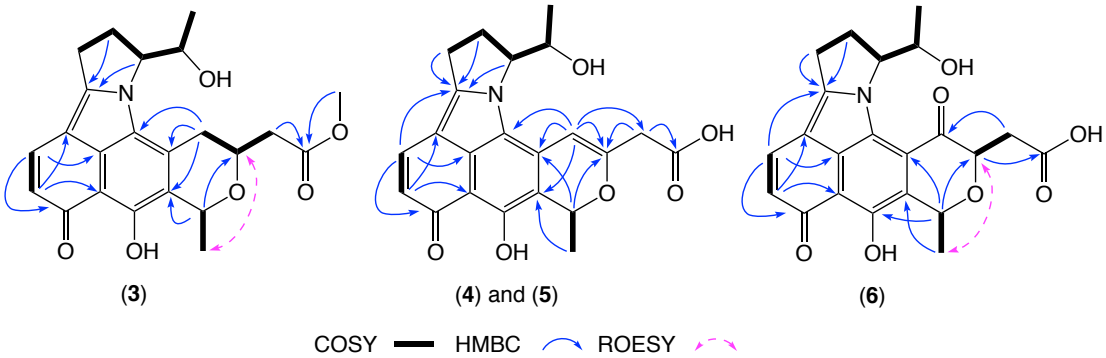

Figure 4. Selected 2D NMR (DMSO-d_6) correlations for **3–6**.

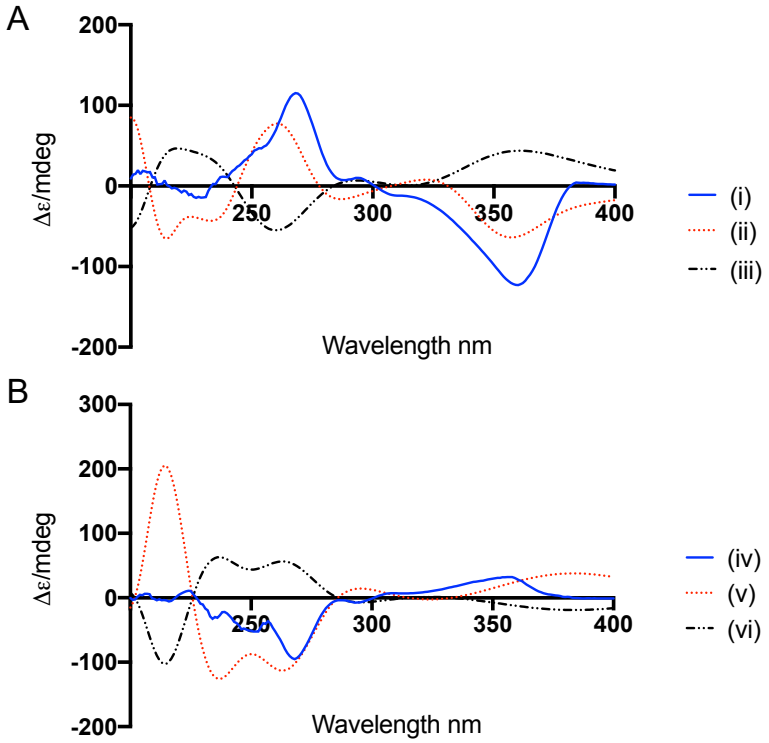

Figure 5. A: Experimental CD spectrum for (i) **4**, and calculated ECD spectrum for (ii) **4A** (4*S*,11*S*,16*R*) and (iii) **4B** (4*R*,11*R*,16*S*); B: Experimental CD spectrum for (iv) **5**, and calculated ECD spectrum for (v) **5A** (4*R*,11*S*,16*R*) and (vi) **5B** (4*S*,11*R*,16*S*).

Table 1. ^{1}H NMR (DMSO-d_6) Data for Glenthenamines A–D (**3–6**)

Pos.	**3**	**4**	**5**	**6**
	δ_H, mult (*J* in Hz)	δ_H, mult (*J* in Hz)	δ_H, mult (*J* in Hz)	δ_H, mult (*J* in Hz)
1	*a*. 3.19, m	6.13, br s	6.23, br s	-
	b. 2.97, dd (16.4, 10.5)	-	-	-
2	4.51, m	-	-	5.11, dd (6.7, 4.3)
4	5.16, q (6.6)	5.80, q (6.6)	5.77, q (6.6)	5.42, q (6.6)
7	6.43, d (9.3)	6.44, d (9.2)	6.44, d (9.3)	6.50, d (9.0)
8	7.96, d (9.3)	7.92, d (9.2)	7.93, d (9.3)	8.09, d (9.0)
9	*a*. 3.20, m	*a*. 3.18, m	*a*. 3.18, m	*a*. 3.26, dd (18.6, 9.7)
	b. 3.13, dd (17.7, 9.2)	*b*. 3.14, m	*b*. 3.14, m	*b*. 3.20, m
10	*a*. 2.67, m	2.68, m	2.68, m	*a*. 2.64, m
	b. 2.63, m			*b*. 2.62, m
11	4.69, br d (8.0)	4.77, br d (7.2)	4.82, br d (8.0)	5.12, br d (6.0)
13	*a*. 2.83, dd (15.8, 4.5)	*a*. 3.43, d (16.5)	*a*. 3.38, d (16.6)	*a*. 2.91, dd (16.5, 4.2)
	b. 2.58, dd (15.8, 8.3)	*b*. 3.30, d (16.5)	*b*. 3.30, d (16.6)	*b*. 2.74, dd (16.5, 6.7)
15	1.53, d (6.6)	1.41, d (6.6)	1.39, d (6.6)	1.67, d (6.7)
16	4.16, qd (6.5, 0.8)	4.13, q (6.6)	4.09, dd (6.6, 1.2)	4.01, qd (6.4, 1.1)
17	1.21, d (6.5)	1.25, d (6.6)	1.22, d (6.6)	1.19, d (6.4)
$OC\underline{H}_3$	3.66, s	-	-	-

HRESI(+)MS measurements on **7** revealed a molecular formula ($C_{20}H_{21}NO_7$, Δmmu +2.8) requiring 11 double bond equivalents. While comparison of the 1D NMR (DMSO-d_6) data for **7** with **1** revealed many similarities, particularly about rings A–D, a principal difference was the absence of the ring E secondary methyl. Diagnostic 2D NMR correlations supported the proposition that **7** shared the ring A–D motif in common with **1**, and the absence of ring E (Tables 3–4 and S9, Figures 6 and S43–S48). Given the above, and consideration of a common biosynthetic pathway, we propose that glenthenamine E (**7**) has the structure as shown, and an absolute configuration in common with co-metabolites **1–2**.

Table 2. ^{13}C NMR (DMSO-d_6) Data for Glenthenamines A–D (**3–6**)

Pos.	**3**	**4**	**5**	**6**
	δ_C, type	δ_C, type	δ_C, type	δ_C, type
1	30.0, CH_2	97.3, CH	98.2, CH	194.9, C
2	62.8, CH	154.9, C	154.5, C	71.1, CH
4	67.4, CH	69.7, CH	70.1, CH	66.7, CH
4a	119.7, C	110.4, C	111.2, C	127.5, C
5	155.5, C	154.5, C	154.6, C	153.8, C
5a	109.7, C	110.5, C	110.4, C	113.8, C
5b	129.4, C	131.0, C	130.9, C	131.1, C
6	185.0, C	183.3, C	183.5, C	185.7, C
7	121.6, CH	121.6, CH	121.7, CH	121.6, CH
8	135.1, CH	134.8, CH	134.8, CH	137.1, CH
8a	103.8, C	104.5, C	104.4, C	103.7, C
8b	154.8, C	156.1, C	155.9, C	158.3, C
9	24.8, CH_2	25.0, CH_2	25.0, CH_2	25.2, CH_2
10	27.5, CH_2	27.0, CH_2	27.0, CH_2	26.0, CH_2
11	64.2, CH	64.5, CH	64.5, CH	67.5, CH
12a	122.0, C	117.4, C	117.5, C	121.2, C
12b	127.2, C	123.5, C	123.2, C	119.8, C
13	40.1, CH_2	40.3, CH_2	40.4, CH_2	36.1, CH_2
14	171.1, C	170.6, C	170.4, C	171.6, C
15	19.5, CH_3	19.9, CH_3	19.6, CH_3	17.7, CH_3
16	68.8, CH	68.1, CH	68.0, CH	68.7, CH
17	20.3, CH_3	20.3, CH_3	20.4, CH_3	20.2, CH_3
O<u>C</u>H_3	51.4, CH_3			

HRESI(+)MS measurements on **8** revealed a molecular formula ($C_{22}H_{23}NO_7$, Δmmu +2.8) suggestive of an oxidized (+O) homologue of **1**. Comparison of the NMR (DMSO-d_6) data for **8** with **1** revealed many similarities, particularly about rings A–D, with the principal difference being deshielding of C-4 and C-4a in **8** (δ_C 96.9, C-4; 139.6, C-4a) compared to **1** (δ_C 67.3, C-4; 119.7, C-4a), consistent with an acetal versus oxymethine carbon (Tables 3–4 and S10, Figures 6 and S49–S54). This hypothesis

was supported by diagnostic 2D NMR correlations which included a ROESY correlation between co-facial H-2 and H_3-15. Given the conserved configuration of the C-4 secondary methyl relative to H-2, we speculate that glenthenamine F (**8**) shares a common absolute configuration with co-metabolites **1–2**.

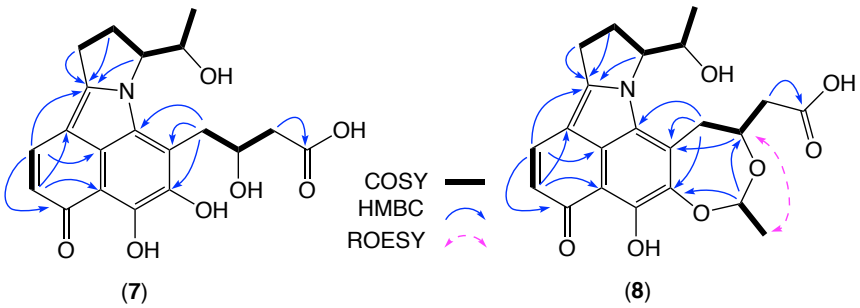

(**7**) (**8**)

Figure 6. Selected 2D NMR (DMSO-d_6) correlations for **7–8**.

A 2017 report describes the biosynthesis of **2** as a traditional Type II polyketide synthase (PKS) assembly of the core framework (rings C–E) with post-PKS C-glycosylation with a deoxyaminosugar.[7] Although this 2017 account suffered from inconsistent and incorrect stereochemical representations of both **2** and biosynthetic intermediates, leading to an incorrect assignment of D-forosamine as the deoxyaminosugar biosynthetic precursor, the underlying premise of a PKS *C*-deoxyaminosugar glycosylation pathway is valid. Building on this, we propose a chemically plausible and stereochemically consistent series of biosynthetic transformations from the *C*-glycoside precursor (i) through the intermediates (ii–vi) to the enamino-pyrrolidine motif evident in **1–8** (Figure 7). Significantly, this sequence proceeds with conservation of the C-11/C-16 configuration. Likewise, we propose a sequence of biosynthetic transformations linking ring E in **1** to related motifs in **2–8**, again proceeding with conservation of the C-2/C-4 configuration (Figure 8). Collectively, these

biosynthetic considerations allow the absolute configurations assigned to **1** and **2** by single crystal X-ray analysis, to be extended to **3–8** and the hypothetical biosynthetic precursor, the deoxyaminosugar **9**.

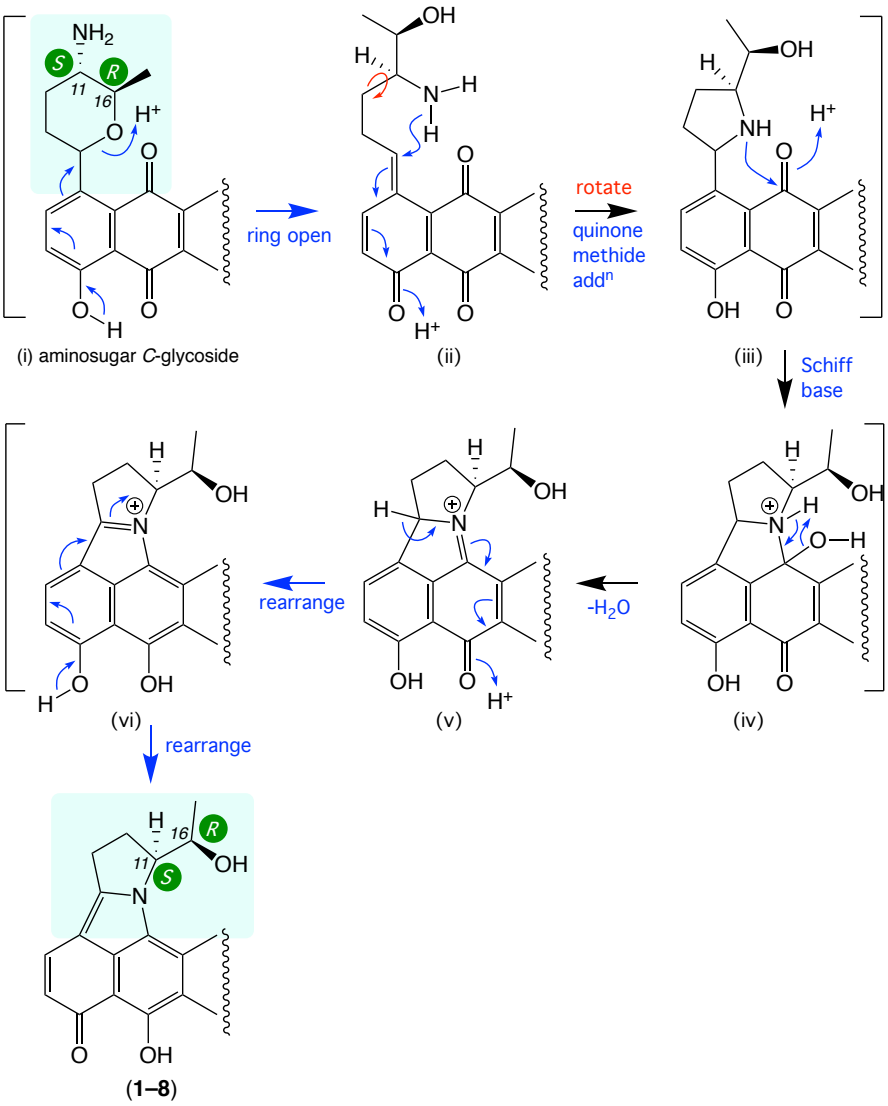

Figure 7. Plausible sequence of biosynthetic transformations linking the deoxyaminosugar *C*-glycosylated precursor (i) to the enamine pyranonaphthoquinones **1–8**, highlighting conservation of configuration about C-11 and C-16.

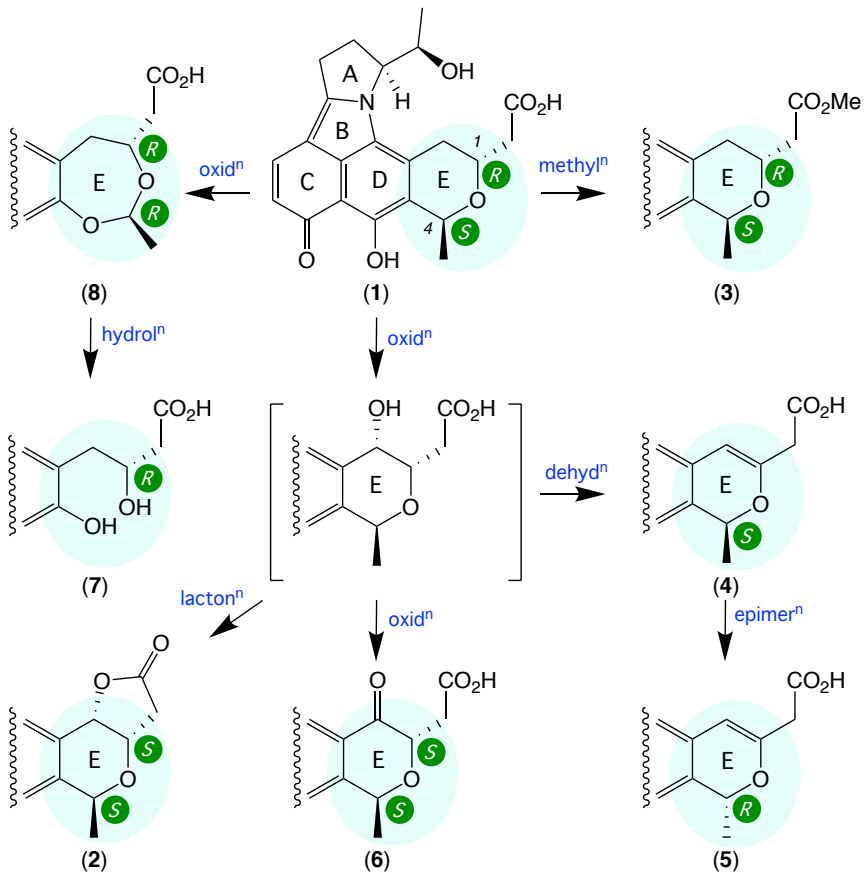

Figure 8. Plausible sequence of biosynthetic transformations linking the enamine pyranonaphthoquinones **1**–**8**, highlighting conservation of configuration about C-1 and C-4.

Efforts to detect the precursor deoxyaminosugar (*i.e.* **9**) in the culture broth proved challenging, due to its low molecular weight and lack of a UV-vis chromophore. To overcome this limitation, a sample of the ISP2 broth culture inoculated with CMB-PB042 was treated with 2,4-dihydroxybenzaldehyde (2,4-DHB) to effect a rapid *in situ* transformation to Schiff base **10**, which was readily detected in the LCMS by single ion extraction (SIE) (Figures 9 and S64). Although the low levels of **10** detected precluded isolation and spectroscopic characterisation, these analyses are consistent with the

proposed biosynthetic pathway linking **9** to **1-8** (note – the structure and absolute configuration of **9** is tentatively inferred from its biosynthetic relationship to **1–8**).

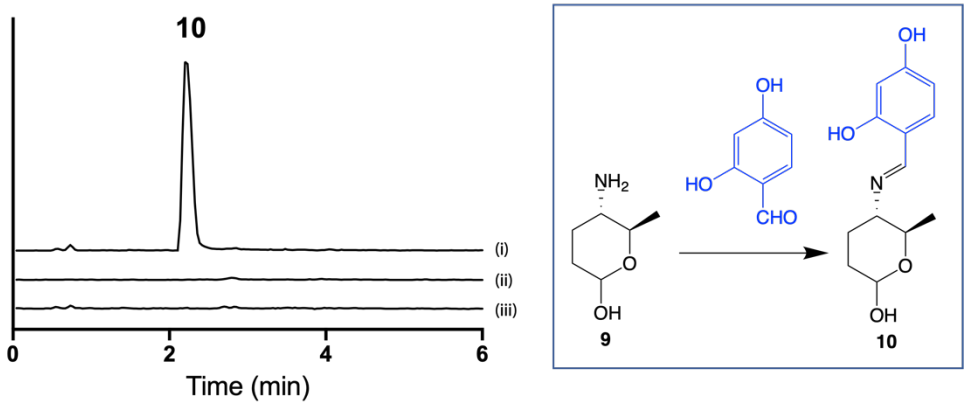

Figure 9. LCMS single ion extraction (SIE) chromatogram at *m/z* 252 of (i) CMB-PB042 broth culture + 2,4-DHB; (ii) ISP-2 medium only + 2,4-DHB; and (iii) CMB-PB042 broth culture only. Inset: Schiff base reaction between the putative precursor **9** with 2,4-DHB.

Table 3. ^{1}H NMR (DMSO-d_6) Data for Glenthenamines E–F (**7–8**)

Pos.	**7** δ_H, mult (*J* in Hz)	**8** δ_H, mult (*J* in Hz)
1	*a*. 3.26, dd (13.1, 4.2)	*a*. 3.55[A]
	b. 2.81, dd (13.1, 9.1)	*b*. 3.24, dd (15.5, 5.9)
2	4.15, m	4.60, m
4	-	5.23, q (5.1)
7	6.41, d (9.1)	6.45, d (9.1)
8	7.93, d (9.1)	7.98, d (9.1)
9	*a*. 3.20, dd (17.8, 8.8)	*a*. 3.20, dd (17.8, 8.9)
	b. 3.12, dd (17.8, 9.0)	*b*. 3.15, ddd (17.8, 9.3, 2.4)
10	*a*. 2.69, dd (12.4, 8.8)	*a*. 2.66, m
	b. 2.59, m	*b*. 2.62, m
11	4.91, br d (8.7)	4.76, br d (8.3)
13	*a*. 2.48, dd, (14.9, 4.1)	*a*. 2.53, dd (15.5, 6.9)
	b. 2.41, dd (14.9, 8.1)	*b*. 2.41, dd (15.5, 7.7)
15	-	1.42, d (5.3)
16	4.11, q (6.5)	4.06, qd (6.4, 1.3)
17	1.24, d (6.5)	1.19, d (6.4)

[A] Resonances obscured by H_2O, but observed by HSQC

Table 4. ^{13}C NMR (DMSO-d_6) Data for Glenthenamines E–F (**7–8**)

Pos.	**7**	**8**
	δ_C, type	δ_C, type
C-1	34.8, CH_2	34.2, CH_2
C-2	67.5, CH	68.4, CH
C-4	-	96.9, CH
C-4a	138.9, C	139.6, C
C-5	147.5, C	151.6, C
C-5a	110.3, C	110.8, C
C-5b	123.4, C	127.0, C
C-6	184.3, C	184.7, C
C-7	120.7, CH	121.4, CH
C-8	134.6, CH	135.1, CH
C-8a	103.8, C	103.7, C
C-8b	154.3, C	156.3, C
C-9	24.8, CH_2	24.7, CH_2
C-10	27.4, CH_2	27.1, CH_2
C-11	63.7, CH	64.2, CH
C-12a	122.0, C	122.3, C
C-12b	123.7, C	126.1, C
C-13	43.0, CH_2	36.8, CH_2
C-14	172.8, C	172.1, C
C-15	-	21.4, CH_3
C-16	68.6, CH	68.2, CH
C-17	20.4, CH_3	20.2, CH_3

In a recent 2020 review, Capon highlighted the sensitivity of some natural products to environmental stimuli, and the importance of distinguishing natural products from artifacts.[9] This concept has featured prominently in some of our recent reports, including the polyketide amaurones from the fish gut-derived fungus *Amauroascus* sp. CMB-F713,[10] the prolinimines and N-amino-L-proline methyl ester from the fish gut-derived fungus *Evlachovaea* sp. CMB-F563,[11, 12] and thorectandrins from the southern Australian marine sponge *Thorectandra choanoides* (CMB-01889).[13] In light of this we were alerted to the possibility that one or more of the glenthenamines may be artifacts. This suspicion was confirmed when UPLC-QTOF single ion extraction (SIE) analysis of fresh EtOAc

extracts from agar plate cultivation of *Streptomyces* sp. CMB-PB042 detected **1–2** and **4–7** but not **3** or **8** (Figure S3). Based on these observations we propose that **3** is a methylation artifact of **1** induced by exposure to MeOH during fractionation and handling, and that **8** is a hydrolysis artifact of **7**, involving loss of an acetaldehyde moiety. Indeed, during storage **8** was observed to undergo partial conversion to **7** (Figure S4).

Compounds **1–8** failed to exhibit significant antimicrobial activity against the Gram-negative bacteria *Escherichia coli* ATCC 11775, the Gram-positive bacteria *Staphylococcus aureus* ATCC 25923, and the fungus *Candida albicans* ATCC 10231 (IC_{50} >30 μM). Likewise, and despite **1–2** being patented in 1998 for the treatment of cancer,[3] in our hands none of **1**–**8** exhibited significant cytotoxic properties (IC_{50} >30 μM) against either human lung (NCI-H460) or colorectal (SW620) carcinoma cells. On the other hand, treatment of P-glycoprotein (P-gp) overexpressing human colon carcinoma cells (SW620 Ad300) with **1** or **3–6** (2.5 μM) reversed doxorubicin resistance with a gain in sensitivity ~45–70% compared to the positive control verapamil (Table 5 and Figure S67). By contrast, **2** and **7–8** were ineffective, highlighting a structure activity requirement for ring E without added ring fusion (i.e. **2**), expansion (i.e. **8**) or cleavage (i.e. **7**).

Table 5. Effect of compounds **1-8** on inhibition of P-gp mediated resistance to doxorubicin in SW620 Ad300

Treatment	IC_{50}[a] (μM)	FR[b]	GS[c]
doxorubicin	5.75	57.5	1.0
+ **1** (2.5 μM)	1.53	15.3	3.7
+ **2** (2.5 μM)	7.58	75.8	0.75
+ **3** (2.5 μM)	1.20	12.0	4.8
+ **4** (2.5 μM)	1.01	10.1	5.7
+ **5** (2.5 μM)	1.44	14.4	3.9
+ **6** (2.5 μM)	1.48	14.8	3.8
+ **7** (2.5 μM)	4.49	44.9	1.28
+ **8** (2.5 μM)	5.04	50.4	1.14
+ verapamil (2.5 μM)	0.71	7.1	8.1
verapamil	>30	NC	NC

[a]MTT assay showing data as means of ± SD of two independent cultures; [b]FR: fold-resistance was determined by dividing the IC_{50} value for doxorubicin for P-gp over-expressing cancer cells by the IC_{50} value for doxorubicin for sensitive cancer cells; [c]GS: Gain in sensitivity was the ratio of IC_{50} value of doxorubicin against SW620 Ad300 without testing compound to IC_{50} value of doxorubicin against SW620 Ad300 with testing compound; NC: not calculated

In conclusion, the antiparasitic property exhibited by a solvent extract of a solid phase culture of the sheep station pasture plant-derived *Streptomyces* sp. CMB-PB042 was attributed to a mixture of known ionophoric polyethers. In this regard GNPS molecular networking proved to be a particularly useful dereplication tool, capable of rapid detection of polyethers, even in complex mixtures. GNPS analysis of CMB-PB042 also revealed a family of highly aromatic nitrogenous metabolites with molecular formulae poorly represented in the natural products literature. Media MATRIX profiling identified optimized conditions, with scaled up cultivation on ISP2 and M2 media yielding the only two known examples of a rare class of enamino pyranonaphthoquinone, BE-54238A (**1**) and BE-54238B (**2**), along with four new natural products, glenthenamines B–D (**4–6**) and F (**8**), and two handling artifacts, glenthenamines A (**3**) and E (**7**). Single crystal X-

ray analyses resolved ambiguities regarding relative and absolute configurations for **1**–**2**, and together with detailed spectroscopic analysis and biosynthetic considerations enabled structures and absolute configurations to be assigned to **3**–**8**. The study of *Streptomyces* sp. CMB-PB042 has greatly expanded knowledge of the chemistry and biological properties of this rare class of enamino pyranonaphthoquinones, including revealing a plausible sequence of biosynthetic transformations linking **1**–**8** with the putative deoxyaminosugar precursor **9**. It has also revealed a new P-gp inhibitory pharmacophore capable of reversing doxorubicin resistance in P-gp overexpressing colon carcinoma cells.

EXPERIMENTAL SECTION

General Experimental Procedures. Chiroptical measurements ($[\alpha]_D$) were obtained on a JASCO P-1010 polarimeter in a 100 × 2 mm cell at specified temperatures. Electronic Circular Dichroism (ECD) measurement were obtained on a JASCO J-810 spectropolarimeter in a 0.1 cm path-length cell. Nuclear magnetic resonance (NMR) spectra were acquired on a Bruker Avance 600 MHz spectrometer with either a 5 mm PASEL ^{1}H/D-^{13}C Z-Gradient probe or 5 mm CPTCI ^{1}H/^{19}F-^{13}C/^{15}N/DZ-Gradient cryoprobe. In all cases spectra were acquired at 25 °C in DMSO-d_6 with referencing to residual ^{1}H or ^{13}C signals (DMSO-d_6, δ_H 2.50 and δ_C 39.5). High-resolution ESIMS spectra were obtained on a Bruker micrOTOF mass spectrometer by direct injection in MeOH at 3 μL/min using sodium formate clusters as an internal calibrant. Liquid chromatography-diode array-mass spectrometry (HPLC-DAD-MS) data were acquired

either on an Agilent 1260 series separation module equipped with an Agilent G6125B series LC/MSD mass detector and diode array detector or on Shimadzu LCMS-2020 LCMS. Semi-preparative HPLCs were performed using Agilent 1100 series HPLC instruments with corresponding detectors, fraction collectors and software inclusively. UPLC chromatograms were obtained on Agilent 1290 infinity UPLC system equipped with diode array multiple wavelength detector (Zorbax C_8 RRHD 1.8 μm, 50 × 2.1 mm column, 0.417 mL/min with a 2.50 min gradient from 90% H_2O/MeCN to MeCN with a constant 0.01% TFA modifier). UPLC-QTOF analysis was performed on UPLC-QTOF instrument comprising an Agilent 1290 Infinity II UPLC (Zorbax C_8 RRHD 1.8 μm, 50 × 2.1 mm column, eluting at 0.417 mL/min with a 2.50 min gradient elution from 90% H_2O/MeCN to 100% MeCN with a constant 0.1% formic acid modifier) coupled to an Agilent 6545 Q-TOF. MS/MS analysis was performed on the same instrument for ions detected in the full scan at an intensity above 1000 counts at 10 scans/s, with an isolation width of 4 ~m/z using a fixed collision energy and a maximum of 3 selected precursors per cycle. Chemicals were purchased from Sigma-Aldrich or Merck unless otherwise specified. Analytical-grade solvents were used for solvent extractions. Chromatography solvents were of HPLC grade supplied by Labscan or Sigma-Aldrich and filtered/degassed through 0.45 μm polytetrafluoroethylene (PTFE) membrane prior to use. Deuterated solvents were purchased from Cambridge Isotopes. Microorganisms were manipulated under sterile conditions using a Laftech class II biological safety cabinet and incubated in either MMM Friocell incubators (Lomb Scientific) or an Innova 42R incubator shaker (John Morris).

Collection and Taxonomy of CMB-PB042. CMB-PB042 was isolated from a sheep pasture plant collected in 2017 near Glenthompson, Australia, using an ISP2 agar plate incubated at 30 °C for 10 days, growing as white back colonies. Genomic DNA was extracted from the mycelia using the DNeasy Plant Mini Kit (Qiagen) as per the manufacturer's protocol. The 16S rRNA genes were amplified by PCR using the universal primers 27F (5′-AGAGTTTGATCCTGGCTCAG-3′) and 1492R (5′-TACGGCTACCTTCTTAC GACTT-3′) purchased from Sigma-Aldrich. The PCR mixture (50 μL) contained genomic DNA (2 μL, 20–40 ng), EmeraldAmpn GT PCR Master Mix (2XPremix) (25 μL), primer (0.2 μM, each), and H_2O (up to 50 μL). PCR was performed using the following conditions: initial denaturation at 95 °C for 2 min, 40 cycles in series of 95 °C for 20 s (denaturation), 56 °C for 20 s (annealing) and 72 °C for 30 s (extension), followed by one cycle at 72 °C for 5 min. The PCR products were purified with PCR purification kit (Qiagen) and sequenced. BLAST analysis (NCBI database) showed that the amplified 16S rRNA sequence (Accession number: MW308307) has 98.9% identity with *Streptomyces* sp. (Figure S1–S2).

Global Natural Product Social (GNPS) Molecular Networking. Aliquots (1 μL) of extracts or fractions (100 μg/mL in MeOH) were analysed on an Agilent 6545 Q-TOF LC/MS equipped with an Agilent 1290 Infinity II UPLC system, utilising an Agilent SB-C8 1.8 μm, 2.1 × 50 mm column, eluting with 90% H_2O/MeCN to MeCN at a 0.417 mL/min over 2.5 min with an isocratic 0.1% formic acid modifier. UPLC-QTOF-(+)MS/MS data acquired for all samples at collision energy of 35 eV were converted from Agilent MassHunter data files (.d) to mzXML file format using MSConvert software, and

transferred to the GNPS server (gnps.ucsd.edu). Molecular networking was performed using the GNPS data analysis workflow[1] using the spectral clustering algorithm with a cosine score of 0.7 and a minimum of 6 matched peaks. The resulting spectral network was imported into Cytoscape version 3.7.1[14] and visualized using a ball-stick layout where nodes represent parent mass and cosine score was reflected by edge thickness. Also, group abundances were set as pie charts, which reflected the intensity of MS signals.

Media MATRIX analysis of CMB-PB042. CMB-PB042 was cultured in a microbioreactor format under 12 different media in solid phase, as well as static and shaken broths (media MATRIX). After 7 days, individual cultivations were extracted with EtOAc (2 mL) and concentrated to dryness under N_2 at 40°C. Individual extracts were redissolved in 100 μL MeOH (comprising of the internal standard 1-decyloxy-2,4-dinitrobenzene, 50 μg/mL) and aliquots (1 μL) subjected to UPLC-DAD analysis (Zorbax C_8 column 1.8 μm, 2.1 × 50 mm column, 0.417 mL/min gradient elution over 2.52 min from 90% H_2O/MeCN to 100% MeCN followed by an isocratic elution for 0.83 min with MeCN, with an isocratic 0.01% TFA modifier).

Scale up Cultivation and Fractionation CMB-PB042.

Cultivation #1: A seed culture of CMB-PB042 was prepared by inoculating a flask (250 mL) containing ISP2 broth medium (80 mL) with several CMB-PB042 colony, followed by incubating at 30 °C with shaking (190 rpm) for 5 days. Aliquots of the seed culture (100 μL) were streaked on to individual ISP2 agar plates (×300) which were then incubated at 30 °C for 14 days. After incubation the agar was diced (~ 1.5 cm × 1.5 cm), transferred to flasks (2 L) and extracted with EtOAc (3 × 500 mL), with the decanted organic layer concentrated *in vacuo* to yield an extract (2.1g). The extract was subjected

to sequential trituration to afford (after drying under nitrogen at 40 °C) *n*-hexane (890 mg) and MeOH (1.28 g) solubles. The MeOH solubles were subjected to preparative reverse-phase HPLC-DAD (Phenomenex Luna-C_8 10 μm, 21.2 × 250 mm column, 20 mL/min gradient elution over 20 min from 80% H_2O/MeCN to 35% H_2O/MeCN, with a constant 0.01% TFA modifier) to yield **1** (50 mg, 2.4%), **2** (20 mg, 1.0%), **3** (3 mg, 0.14%) and 30 other fractions. Fractions 21 (31.2 mg), 22 (35.5 mg) and 23 (25 mg) were subjected to further semi-preparative HPLC-DAD (Zorbax C_{18} 5 μm, 250 × 9.4 mm column, 3 mL/min gradient elution over 20 min from 75% H_2O/MeCN to 65% H_2O/MeCN, with a constant 0.01% TFA modifier to yield **4** (4.0 mg, 0.19%) and **5** (4.0 mg, 0.19%); Fraction 15 (24.1 mg) was subjected to semi-preparative HPLC (Zorbax C_{18} 5 μm, 250 × 9.4 mm column, 3 mL/min gradient elution over 20 min from 85% H_2O/MeCN to 50% H_2O/MeCN, with a constant 0.01% TFA modifier to yield **7** (2.2 mg, 0.11%), **8** (4.3 mg, 0.21%).

Cultivation #2: A selection of M2 agar plates (×100) were inoculated, cultivated and extracted as detailed above to generate an extract (380 mg) that was dissolved in MeOH (1.5 mL) and centrifuged, after which the supernatant was subjected to gel chromatography (Sephadex LH20, MeOH) followed by semi-preparative HPLC-DAD (Zorbax C_{18} 5 μm, 250 × 9.4 mm column, 3 mL/min gradient elution over 25 min from 90% H_2O/MeCN to 45% H_2O/MeCN with a constant 0.01% TFA modifier) to yield **6** (2.2 mg, 0.58%). (Note: All % yields are weight to weight estimates based on unfractionated EtOAc extract)

*BE-54238A (**1**)*: yellowish needles; $[\alpha]^{22}_D$ -385 (*c* 0.03, MeOH); 1D and 2D NMR (DMSO-d_6), Tables S3; HRESIMS *m/z* 398.1615 $[M + H]^+$ (calcd for $C_{22}H_{24}NO_6$,

398.1598).

*BE-54238B (**2**)*: yellowish needles; $[\alpha]^{22}_{D}$ -323 (*c* 0.02, MeOH); 1D and 2D NMR (DMSO-d_6), Tables S4; HRESIMS *m/z* 396.1466 $[M + H]^+$ (calcd for $C_{22}H_{22}NO_6$, 396.1442).

*Glenthenamine A (**3**)*: yellowish powder; $[\alpha]^{22}_{D}$ -254 (*c* 0.02, MeOH); 1D and 2D NMR (DMSO-d_6), Tables 1, 2, and S5; HRESIMS *m/z* 412.1777 $[M + H]^+$ (calcd for $C_{23}H_{26}NO_6$, 412.1755).

*Glenthenamine B (**4**)*: yellowish powder; $[\alpha]^{22}_{D}$ -567 (*c* 0.03, MeOH); 1D and 2D NMR (DMSO-d_6), Tables 1, 2, and S6; HRESIMS *m/z* 396.1468 $[M + H]^+$ (calcd for $C_{22}H_{22}NO_6$, 396.1442).

*Glenthenamine C (**5**)*: yellowish powder; $[\alpha]^{22}_{D}$ -40 (*c* 0.02, MeOH); 1D and 2D NMR (DMSO-d_6), Tables 1, 2, and S7; HRESIMS *m/z* 396.1467 $[M + H]^+$ (calcd for $C_{22}H_{22}NO_6$, 396.1442).

*Glenthenamine D (**6**)*: orange powder; $[\alpha]^{22}_{D}$ -265 (*c* 0.02, MeOH); 1D and 2D NMR (DMSO-d_6), Tables 1, 2, and S8; HRESIMS *m/z* 412.1401 $[M + H]^+$ (calcd for $C_{22}H_{22}NO_7$, 412.1391).

*Glenthenamine E (**7**)*: yellowish powder; $[\alpha]^{22}_{D}$ -158 (*c* 0.02, MeOH); 1D and 2D NMR (DMSO-d_6), Tables 3, 4, and S9; HRESIMS *m/z* 388.1419 $[M + H]^+$ (calcd for $C_{20}H_{22}NO_7$, 388.1391).

*Glenthenamine F (**8**)*: yellowish powder; $[\alpha]^{22}_{D}$ -241 (*c* 0.01, MeOH); 1D and 2D NMR (DMSO-d_6), Tables 3, 4, and S10; HRESIMS *m/z* 414.1575 $[M + H]^+$ (calcd for $C_{22}H_{24}NO_7$, 414.1547).

X-ray Crystallography. Crystals of **1** and **2** were obtained by slow evaporation from 50% aqueous MeCN at room temperature. Crystallographic data (CuKα radiation 1.54184 Å, 2θmax = 125°) were collected on an Oxford Diffraction Gemini S Ultra CCD diffractometer with the crystal cooled to 190 K with an Oxford Cryosystems Desktop Cooler. Data reduction and empirical absorption corrections were carried out with the CrysAlisPro program (Oxford Diffraction vers. 171.38.46). The structure was solved by direct methods with SHELXT and refined with SHELXL.[15] The thermal ellipsoid diagrams were generated with Mercury.[16] All crystallographic calculations were carried out within the WinGX graphical user interface.[17] The crystal structures for **1** and **2** have been deposited in the CCDC database (CCDC 2084059 and CCDC 2084060, respectively).

ECD calculations. Monte Carlo conformational searches were carried out by means of the Spartan's 14 software using Merck Molecular Force Field (MMFF).[18] The conformers with Boltzmann-population of over 5% were chosen for ECD calculations, and then the conformers were initially optimized at B3LYP/6-31g level in gas. The theoretical calculation of ECD was conducted in MeOH using Time-dependent Density functional theory (TD-DFT) at the B3LYP/6-31+g (d, p) level for the conformers of compounds **4A**, **4B**, **5A** and **5B**. Rotatory strengths for a total of 30 excited states were calculated. ECD spectra were generated using the program SpecDis 1.6 (University of Würzburg, Würzburg, Germany) and GraphPad Prism 5 (University of California San Diego, USA) from dipole-length rotational strengths by applying Gaussian band shapes with sigma = 0.3 eV.

Detection of deoxyaminosugar 9 using 2,4-dihydroxybenzaldehyde. An aliquot (40 μL) of 2,4-dihydroxybenaldehyde (2,4-DHB, 5 mg/mL in 20% aqueous DMSO) was added to a 7d culture of CMB-PB042 in ISP2 broth (1.5 mL). After shaking for 30 min, the solution was extracted with EtOAc (2 mL). The organic layer was dried under N_2 flow at room temperature, and the resulting extract redissolved in MeOH (200 μL) and subjected to LC-MS analysis to detect **10** (Figure 9). EtOAc extracts of CMB-PB042 grown in ISP2 broth (1.5 mL) without addition of 2,4-DHB, and uninoculated ISP2 broth (1.5 mL), were used as negative controls.

Antiparasitic Assays. Antiparasitic assays were performed by the industry partner Boehringer Ingelheim using commercial-in-confidence protocols.

Antibiotic Assays. Antibacterial and antifungal assays were performed using prior published methods,[10] as documented in the Supporting Information (Section 10).

Cytotoxicity Assays. Cytotoxicity assays were performed using prior published methods,[10] as documented in the Supporting Information (Section 11).

P-gp Inhibition and Reversal of Doxorubicin Resistance Assay. Assays were performed using prior published methods,[19, 20] as documented in the Supporting Information (Section 12).

SUPPORTING INFORMATION

The Supporting Information is available free of charge on the ACS Publication website at DOI: ######

Bacterial taxonomy, NMR spectra and tabulated NMR data for **1**-**8**, bioassay methods and results, ECD calculations, and X-Ray crystallographic data (PDF).

AUTHOR INFORMATION

Corresponding Authors

E-mail: r.capon@uq.edu.au Phone +61 7 3346 2979

Notes

The authors declare no competing financial interest.

ACKNOWLEDGMENTS

The authors thank K. Agnew and participating pastoralists for assistance in sourcing pasture samples from sheep properties across Australia, Y. Moreno and Boehringer Ingelheim for antiparasitic assays, and S. Bates and R. Robey (NCI) for providing the SW620 Ad300 cell line. T. Wu thanks The University of Queensland for an International Postgraduate Scholarship. This work was funded in part by the Institute for Molecular Bioscience, The University of Queensland, and Boehringer Ingelheim.

REFERENCES

1. Wang, M.; Carver, J. J.; Phelan, V. V.; Sanchez, L. M.; Garg, N.; Peng, Y.; Nguyen, D. D.; Watrous, J.; Kapono, C. A.; Luzzatto-Knaan, T.; Porto, C.; Bouslimani, A.; Melnik, A. V.; Meehan, M. J.; Liu, W.-T.; Crüsemann, M.; Boudreau, P. D.; Esquenazi, E.; Sandoval-Calderón, M.; Kersten, R. D.; Pace, L. A.; Quinn, R. A.; Duncan, K. R.; Hsu, C.-C.; Floros, D. J.; Gavilan, R. G.; Kleigrewe, K.; Northen, T.; Dutton, R. J.; Parrot, D.; Carlson, E. E.; Aigle, B.; Michelsen, C. F.; Jelsbak, L.; Sohlenkamp, C.; Pevzner, P.; Edlund, A.; McLean, J.; Piel, J.; Murphy, B. T.; Gerwick, L.; Liaw, C.-C.; Yang, Y.-L.; Humpf, H.-U.; Maansson, M.; Keyzers, R. A.; Sims, A. C.; Johnson, A. R.; Sidebottom, A. M.; Sedio, B. E.; Klitgaard, A.; Larson, C. B.; Boya P, C. A.; Torres-Mendoza, D.; Gonzalez, D. J.; Silva, D. B.; Marques, L. M.; Demarque, D. P.; Pociute, E.; O'Neill, E. C.; Briand, E.; Helfrich, E. J. N.; Granatosky, E. A.; Glukhov, E.; Ryffel, F.; Houson, H.; Mohimani, H.; Kharbush, J. J.; Zeng, Y.; Vorholt, J. A.; Kurita, K. L.; Charusanti, P.; McPhail, K.

L.; Nielsen, K. F.; Vuong, L.; Elfeki, M.; Traxler, M. F.; Engene, N.; Koyama, N.; Vining, O. B.; Baric, R.; Silva, R. R.; Mascuch, S. J.; Tomasi, S.; Jenkins, S.; Macherla, V.; Hoffman, T.; Agarwal, V.; Williams, P. G.; Dai, J.; Neupane, R.; Gurr, J.; Rodríguez, A. M. C.; Lamsa, A.; Zhang, C.; Dorrestein, K.; Duggan, B. M.; Almaliti, J.; Allard, P.-M.; Phapale, P.; Nothias, L.-F.; Alexandrov, T.; Litaudon, M.; Wolfender, J.-L.; Kyle, J. E.; Metz, T. O.; Peryea, T.; Nguyen, D.-T.; VanLeer, D.; Shinn, P.; Jadhav, A.; Müller, R.; Waters, K. M.; Shi, W.; Liu, X.; Zhang, L.; Knight, R.; Jensen, P. R.; Palsson, B. Ø.; Pogliano, K.; Linington, R. G.; Gutiérrez, M.; Lopes, N. P.; Gerwick, W. H.; Moore, B. S.; Dorrestein, P. C.; Bandeira, N. *Nat. Biotechnol* **2016,** *34*, 828-837.

2. Dewapriya, P.; Khalil, Z. G.; Prasad, P.; Salim, A. A.; Cruz-Morales, P.; Marcellin, E.; Capon, R. J. *Front. Chem.* **2018,** *6*, 394.
3. Tsukamoto, M.; Nakajima, S.; Nagashima, M.; Ojiri, K.; Suda, H. JPH10-59975, 1998.
4. Tsukamoto, M.; Nakajima, S.; Murooka, K.; Hirayama, M.; Hirano, K.; Yoshida, S.; Kojiri, K.; Suda, H. *J Antibiot.* **2000,** *53*, 26-32.
5. Tatsuta, K.; Hirabayashi, T.; Kojima, M.; Suzuki, Y.; Ogura, T. *J Antibiot.* **2004,** *57*, 291-297.
6. Tatsuta, K.; Hosokawa, S. *Chem. Rec.* **2006,** *6*, 217-233.
7. Wu, C.; Du, C.; Ichinose, K.; Choi, Y. H.; van Wezel, G. P. *J. Nat. Prod.* **2017,** *80*, 269-277.
8. Hooft, R. W. W.; Straver, L. H.; Spek, A. L. *J. Appl. Crystallogr.* **2008,** *41*, 96-103.
9. Capon, R. J. *Nat. Prod. Rep.* **2020,** *37*, 55-79.
10. Wu, T.; Salim, A. A.; Bernhardt, P. V.; Capon, R. J. *J. Nat. Prod.* **2021,** *84*, 474-482.
11. Mohamed, O. G.; Khalil, Z. G.; Capon, R. J. *Org. Lett.* **2018,** *20*, 377-380.
12. Mohamed, O. G.; Khalil, Z. G.; Capon, R. J. *Mar. Drugs* **2021,** *19*, 151.
13. Khushi, S.; Salim, A. A.; Elbanna, A. H.; Nahar, L.; Capon, R. J. *Mar. Drugs* **2021,** *19*, 97.
14. Shannon, P.; Markiel, A.; Ozier, O.; Baliga, N. S.; Wang, J. T.; Ramage, D.; Amin, N.; Schwikowski, B.; Ideker, T. *Genome Res.* **2003,** *13*, 2498-2504.
15. Sheldrick, G. M. *Acta Crystallogr. A.* **2008,** *64*, 112-122.
16. Macrae, C. F.; Edgington, P. R.; McCabe, P.; Pidcock, E.; Shields, G. P.; Taylor, R.; Towler, M.; van de Streek, J. *J. Appl. Crystallogr.* **2006,** *39*, 453-457.
17. Farrugia, L. *J. Appl. Crystallogr.* **1999,** *32*, 837-838.
18. Li, H. L.; Li, X. M.; Mándi, A.; Antus, S.; Li, X.; Zhang, P.; Liu, Y.; Kurtán, T.; Wang, B. G. *J. Org. Chem.* **2017,** *82*, 9946-9954.
19. Elbanna, A. H.; Khalil, Z. G.; Bernhardt, P. V.; Capon, R. J. *Org. Lett.* **2019,** *21*, 8097-8100.
20. Mohamed, O. G.; Salim, A. A.; Khalil, Z. G.; Elbanna, A. H.; Bernhardt, P. V.; Capon, R. J. *J. Nat. Prod.* **2020,** *83*, 497-504.

TOC graphical abstract